Supplementary Material *for* Strain-Induced Quasi-1D Channels in Twisted Moiré Lattices

Andreas Sinner,[1,2,*] Pierre A. Pantaleón,[1,†] and Francisco Guinea[1,3,4]

[1] *IMDEA Nanoscience, Faraday 9, 28049 Madrid, Spain*
[2] *Institute of Physics, University of Opole, 45-052 Opole, Poland*
[3] *Donostia International Physics Center, Paseo Manuel de Lardizábal 4, 20018 San Sebastián, Spain*
[4] *Ikerbasque, Basque Foundation for Science, 48009 Bilbao, Spain*

CONTENTS

I. STRAIN INDUCED QUASI-UNIDIMENSIONAL CHANNELS

Figure S1 shows a twisted bilayer moiré lattice under strain. The relative angle between honeycomb lattices is set to be 3° for better visualization of the stacking and emergent patterns. The stacking configuration is set to AA at the origin. Figure S1a) shows the case of $-\epsilon_{yy}/\epsilon_{xx} = 0.165$ (graphene Poisson ratio), b) of $-\epsilon_{yy}/\epsilon_{xx} = 1/3$ and c) of $-\epsilon_{yy}/\epsilon_{xx} = 1/12$. The periodicity reveals quasi-unidimensional channels with an AA stacking configuration. A detailed analysis of the distorted lattice vectors which lead to these patterns will be presented later. However, as explained in the main text, the relaxation of the atomic sites shrinks significantly these AA regions giving rise to unidimensional channels [1].

II. CRITICAL STRAIN AND TWIST ANGLE

Figure S2a) shows the critical strain percentage as a function of the twist angle, cf. Eq. (6) in the main text. As the twist angle is reduced, the strain required to form unidimensional channels becomes smaller. Figure S2a) shows the magnitude of the moiré length as a function of the strain parameter for different twist angles. Additionally, we have included two animations, "TwistVariation.mp4" (animation 1) and "StrainVariation.mp4" (animation 2), which depict the variation of the unit cell in both real and reciprocal space. For both animations, in a) the black hexagon is the real space unit cell and the arrows the lattice vectors. In b) we display the Brillouin zone of each monolayer in blue and red, respectively. Colored arrows are the corners of each Brillouin zone and the black black arrows connecting them are the corresponding differences which are used to construct the moiré Brillouin zone shown in c). In animation 1,

* andreas.sinner@uni.opole.pl

† ppantaleon@uabc.edu.mx

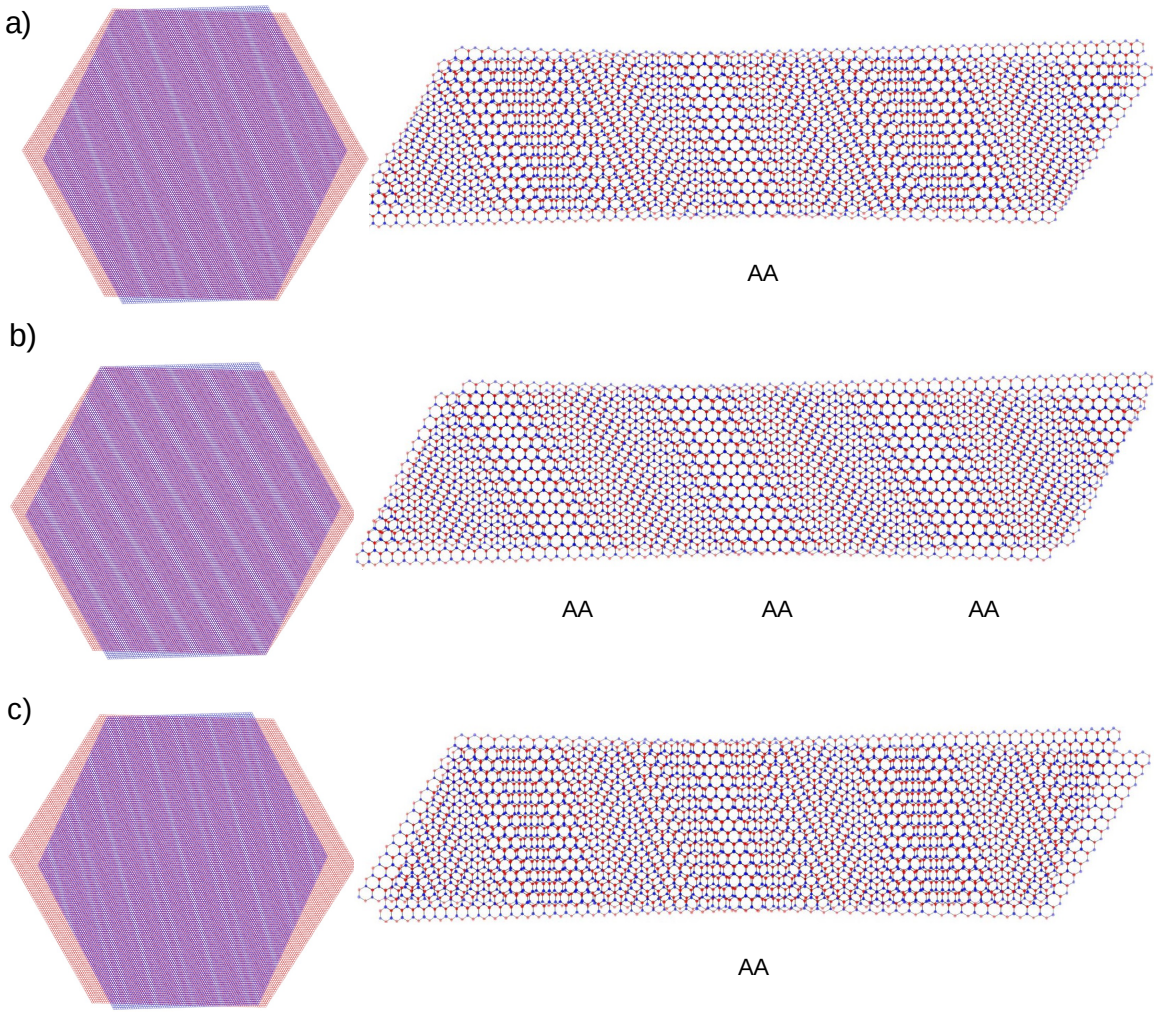

FIG. S1. Strain induced quasi-unidimensional channels in the twisted bilayer moiré lattice. The twist angle is chosen at 3.0° and the strain parameter is $x = 1$ in all figures. The ratio between the applied heterostrain is a) $-\epsilon_{yy}/\epsilon_{xx} = 0.165$, b) $-\epsilon_{yy}/\epsilon_{xx} = 1/3$ and c) $-\epsilon_{yy}/\epsilon_{xx} = 1/12$. Figures on the right are enlarged cuts to visualize the stack configuration for each strain ratio. The AA stacking centers are indicated.

we modify the twist angle while keeping the strain at zero to observe the behavior of the lattice vectors. We consider only commensurate solutions, and the corresponding real and reciprocal unit cells are shown in each panel. Animation 2 focuses on a fixed twist angle (which we set to $\theta = 5.09°$ to better visualize the moiré) while varying the strain magnitude. For this animation, we do not strictly consider a commensurate situation. A description of this case can be found in the following section. In animation 2, as we approach the critical strain, the lattice vectors are enlarged. The values on the top of panel (a) represent the applied strain value for $\theta = 5.09°$. For comparison, colored in red, we also provide the corresponding strain magnitude for $\theta = 1.0°$.

III. CRITICAL STRAIN CONDITION FOR A COMMENSURATE STRUCTURE AND LOW TWIST ANGLE

As mentioned in the main text, a bilayer at the critical heterostrain is characterized by a transformation matrix $\mathbf{T}$ given (in the small angle, small strain limit, $\theta, \epsilon_{xx}, \epsilon_{yy} \ll 1$) by :

$$\mathbf{T} = \begin{pmatrix} \epsilon_{xx}\cos^2(\phi) + \epsilon_{yy}\sin^2(\phi) & -\theta + (\epsilon_{xx} - \epsilon_{yy})\sin(\phi)\cos(\phi) \\ \theta + (\epsilon_{xx} - \epsilon_{yy})\sin(\phi)\cos(\phi) & \epsilon_{xx}\sin^2(\phi) + \epsilon_{yy}\cos^2(\phi) \end{pmatrix}, \tag{S1}$$

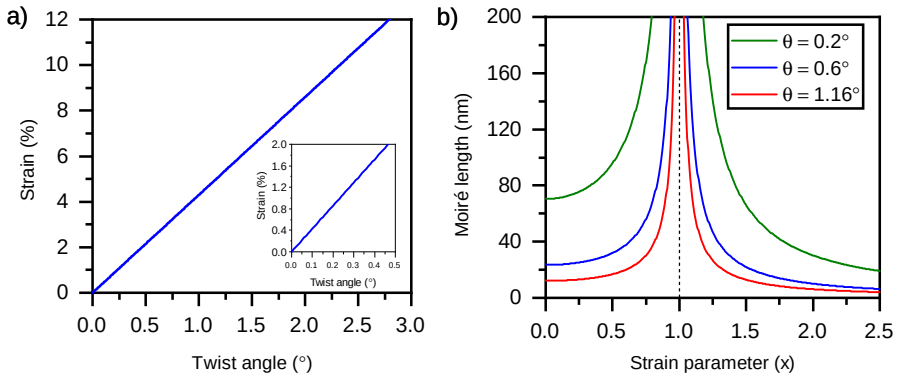

FIG. S2. a) Critical strain as function of the twist angle, cf. Eq. (6) in the main text. For smaller twist angles (inset) the critical strain is within the experimental range. b) Moiré length versus strain parameter x at different twist angles. At the critical point the moiré length diverges resulting in uni-dimensional channels in real space. Notice that after the critical point at $x = 1$ is passed, the unit cell is again well defined.

where $\epsilon_{xx}, \epsilon_{yy}$ are the components of the uniaxial strain tensor along some fixed axes of coordinates, and ϕ is the angle with respect to that axis in which the strain is applied. The critical strain condition, $\det|\mathbf{T}| = 0$ implies:

$$\epsilon_{xx}\epsilon_{yy} = -\theta^2. \tag{S2}$$

A more compact way of writing the matrix $\mathbf{T}$ is:

$$\mathbf{T} = 2\begin{pmatrix} \alpha_1 \cos(\bar{\phi}) & \alpha_2 \cos(\bar{\phi}) \\ \alpha_1 \sin(\bar{\phi}) & \alpha_2 \sin(\bar{\phi}) \end{pmatrix}, \tag{S3}$$

where the parameters $\alpha_1, \alpha_2, \bar{\phi}$ can be obtained from $\epsilon_{xx}, \epsilon_{yy}, \theta, \phi$ in Eq. (S1) and the constraint in Eq. (S2). Again, without loss of generality, we can choose three vectors of the real space unperturbed graphene layers as:

$$\begin{aligned} \vec{a}_1 &= d\,\{1, 0\}\,, \\ \vec{a}_2 &= d\left\{-\frac{1}{2}, \frac{\sqrt{3}}{2}\right\}, \\ \vec{a}_3 &= d\left\{-\frac{1}{2}, -\frac{\sqrt{3}}{2}\right\}, \end{aligned} \tag{S4}$$

where d is the lattice constant (in the main text we use a for the lattice constant, here we modified it to avoid confusions with the notation). The distortion of these vectors induced by the twist and strain is:

$$\begin{aligned} \Delta\vec{a}_1 &= \pm d\alpha_1 \left\{\cos(\bar{\phi}), \sin(\bar{\phi})\right\}, \\ \Delta\vec{a}_2 &= \pm d\left(-\frac{\alpha_1}{2} + \frac{\alpha_2\sqrt{3}}{2}\right)\left\{\cos(\bar{\phi}), \sin(\bar{\phi})\right\}, \\ \Delta\vec{a}_3 &= \pm d\left(-\frac{\alpha_1}{2} - \frac{\alpha_2\sqrt{3}}{2}\right)\left\{\cos(\bar{\phi}), \sin(\bar{\phi})\right\}. \end{aligned} \tag{S5}$$

Three vectors in the reciprocal lattice are:

$$\begin{aligned} \vec{g}_1 &= \frac{4\pi}{\sqrt{3}d}\,\{0, 1\}\,, \\ \vec{g}_2 &= \frac{4\pi}{\sqrt{3}d}\left\{\frac{\sqrt{3}}{2}, -\frac{1}{2}\right\}, \\ \vec{g}_3 &= \frac{4\pi}{\sqrt{3}d}\left\{-\frac{\sqrt{3}}{2}, -\frac{1}{2}\right\}. \end{aligned} \tag{S6}$$

The distortions of these vectors are:

$$\Delta\vec{g}_1 = \mp\frac{4\pi}{\sqrt{3}d}\sin(\bar{\phi})\left\{\alpha_1, \frac{\sqrt{3}}{2}\alpha_2\right\},$$
$$\Delta\vec{g}_2 = \mp\frac{4\pi}{\sqrt{3}d}\left(\frac{\sqrt{3}\cos(\bar{\phi})}{2} - \frac{\sin(\bar{\phi})}{2}\right)\left\{\alpha_1, \frac{\sqrt{3}}{2}\alpha_2\right\},$$
$$\Delta\vec{g}_3 = \mp\frac{4\pi}{\sqrt{3}d}\left(-\frac{\sqrt{3}\cos(\bar{\phi})}{2} - \frac{\sin(\bar{\phi})}{2}\right)\left\{\alpha_1, \frac{\sqrt{3}}{2}\alpha_2\right\}. \tag{S7}$$

The results in Eqs. (S5) and (S7) have been obtained from:

$$\vec{a}_j\Delta\vec{g}_i = -\vec{g}_i\Delta\vec{a}_j, \quad i,j = 1,2,3. \tag{S8}$$

This equation is valid to lowest order in $\mathbf{T}$. The set of values $\Delta\vec{a}_i$ and $\Delta\vec{g}_i$ are collinear, and, in the same manner as in a simply twisted bilayer graphene, the moiré superlattice is determined by $\Delta\vec{g}_i$. Note that $\sum_{i=1,2,3}\Delta\vec{a}_i = \sum_{i=1,2,3}\Delta\vec{g}_i = 0$, and only two vectors are independent, as required for a two dimensional lattice. A sketch of the lattice and reciprocal lattice vectors, as well as the unit cell and the Brillouin zone are shown in Fig. S3.

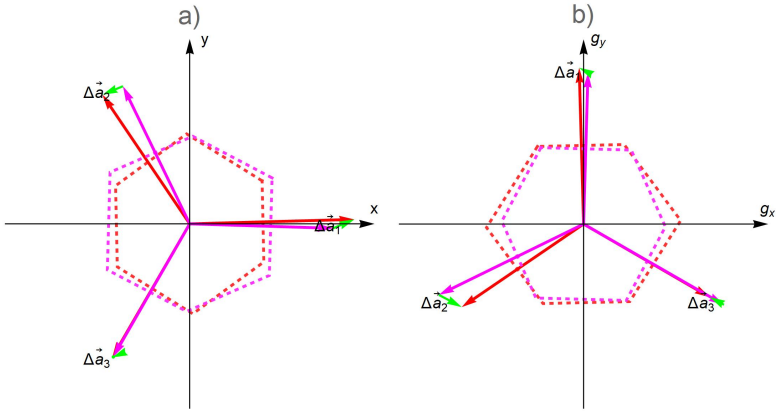

FIG. S3. a) The real space unit cell of the two deformed layers in the bilayer (dashed lines) and lattice vectors (arrows). b) The Brillouin zone of the two deformed layers (dashed lines) and reciprocal lattice vectors (arrows). The differences between reciprocal lattice vectors (green arrows) define the moiré lattice unit vectors. The parameters used are $\{\alpha_1, \alpha_2\} = \{0.075, -0.04\}$ and $\bar{\phi} = \pi/8$.

A moiré superlattice commensurate with the atomic scale lattices of the two layers can be obtained by adjusting the parameters $\alpha_1, \alpha_2, \bar{\phi}$ so that integer multiples of $\Delta\vec{a}_1, \Delta\vec{a}_2, \Delta\vec{a}_3$ coincide with vectors of the real lattice of the unperturbed layers. The choice $\alpha_1 \neq 0, \alpha_2 = 0, \bar{\phi} = 2\pi/3$ gives a one dimensional moiré superlattice, aligned along the $y-$axis of the lattice. We can write the lattice vectors of the two layers as:

$$\vec{a}^t_{m,n} = (\mathcal{I} + \mathbf{T})(m\vec{a}_2 + n\vec{a}_3) = d\left\{-\frac{1}{2}(m+n)\left(1 - \frac{\alpha_1}{2}\right), \frac{\sqrt{3}}{2}(m-n)\left(1 - \frac{\alpha_1}{2}\right)\right\},$$
$$\vec{a}^b_{m,n} = (\mathcal{I} - \mathbf{T})(m\vec{a}_2 + n\vec{a}_3) = d\left\{-\frac{1}{2}(m+n)\left(1 + \frac{\alpha_1}{2}\right), \frac{\sqrt{3}}{2}(m-n)\left(1 + \frac{\alpha_1}{2}\right)\right\}, \tag{S9}$$

where $\mathcal{I}$ is the 2×2 identity matrix, and the t, b indices refer to the top and bottom layers. For rational values of α_1 this distortion defines a commensurate one dimensional moiré lattice, modulated along the $x-$ axis. For instance, for $\alpha_1 = 1/n$, we obtain:

$$(4n-1)\vec{a}^t_2 + (4n+1)\vec{a}^t_3 = (-4n+1)\vec{a}_1$$
$$(4n+1)\vec{a}^b_2 + (4n-1)\vec{a}^b_3 = (-4n-1)\vec{a}_1$$
$$\vec{a}^t_2 - \vec{a}^t_3 = \vec{a}^b_2 - \vec{a}^b_3 = \vec{a}_2 - \vec{a}_3 \tag{S10}$$

These equalities define a commensurate moiré superlattice. The periodicity in the horizontal direction is $\ell_m^{\parallel} = (4n^2-1)d$, and the only periodicity in the vertical direction is the atomic periodicity of the graphene layers, $\ell_m^{\perp} = \vec{a}_2 - \vec{a}_3 = \sqrt{3}d$, as shown in Fig. S4. The vertical periodicity is ignored in the continuum model, which focuses on properties at scales larger than the interatomic distance.
Results for $\alpha_1 = 1/20, \alpha_2 = 0, \bar{\phi} = \arctan(2\pi/3)$ are shown in Fig. S4. It is worth noting that the two patterns show modulations where regions of type AA or AB are present, depending on the center of rotation. The intermediate regions, however, cannot be classified as either AB or AA, unlike in unidimensional moiré lattices defined solely by strains [2–5]. Other non-conmensurate one dimensional patterns are shown in Fig. S1.

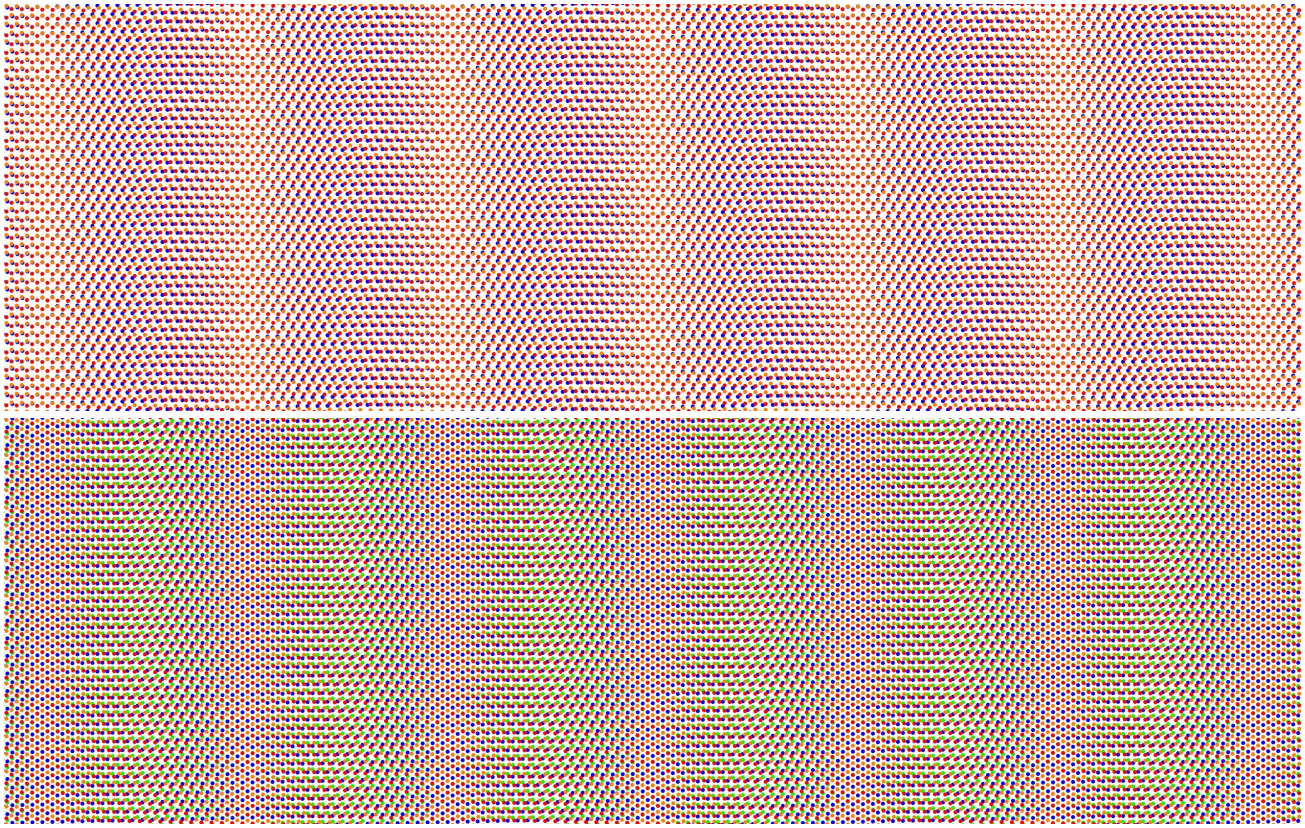

FIG. S4. Critically strained twisted bilayer honeycomb lattice defined by the parameters $\{\alpha_1, \alpha_2, \bar{\phi}\} = \{1/20, 0, 2\pi/3\}$ as described in Sec. III. Top: rotation around an AA region. Bottom: rotation around an AB region. The two sublattices in the top layer are shown as red and orange dots. The two sublattices in the bottom layer are shown as blue and green dots.

IV. EDGE DOMAIN WALLS

Figure S5 shows different domain walls generated by the uniaxial heterostrain of different strength. Black arrows indicate the direction of the strain increasing from zero to a finite value. Each triangle represents an AB/BA domain and the vertices in the triangles are at the position of the AA centers in each unit cell. These domains are constructed from the linear combinations of the lattice vectors defined in Eq. (13) and Eq. (14). Further realizations of deformed systems for various strains can be constructed from distorted hexagons, as for instance those shown in Fig. S5 or Fig. 1g). It is worth noting that inhomogeneites at the atomic scale are magnified in moiré superlattices [6–8]. We leave for later work the study of the interplay between atomic defects, twists, and strains.

V. THE CONTINUUM MODEL OF TBG WITH UNIAXIAL HETEROSTRAIN

In the limit of sufficiently large periods of the moiré superlattices measured with respect to the atomic scale of the monolayer graphene, the physics of TBG is well described by the effective continuum model [9–11]. For strained

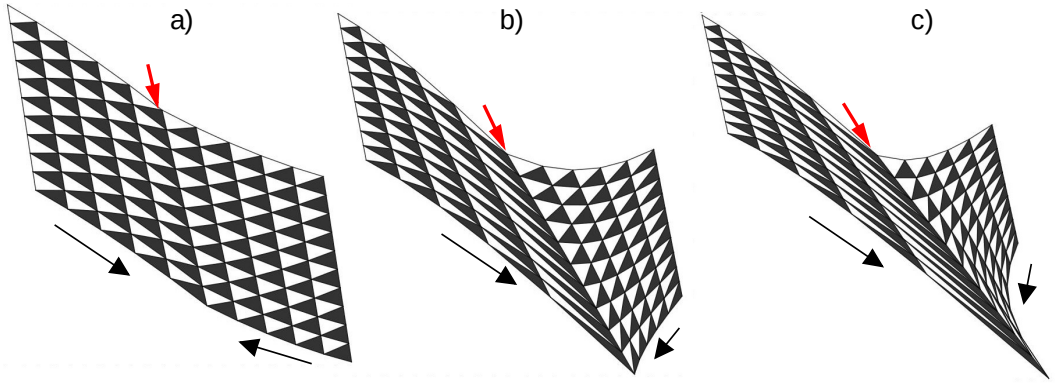

FIG. S5. The visualization of the domain walls formation for different strain values. The non uniform strain increases from zero up to a finite value. At each maximum, there appears a domain wall indicated by red arrows. For each panel this maximal strain is a) $0.3\epsilon_c$, b) $0.6\epsilon_c$ and c) $0.7\epsilon_c$

twisted bilayer graphene the continuum model takes the form

$$H_{\mathrm{TBG}} = \begin{pmatrix} H(\mathbf{q}_\zeta^\uparrow) & U^\dagger(r) \\ U(r) & H(\mathbf{q}_\zeta^\downarrow) \end{pmatrix}. \tag{S11}$$

The diagonal terms describe the Dirac particles in each layer

$$H(\mathbf{q}_\zeta^\ell) = -\hbar v_F \mathbf{q}_\zeta^\ell \cdot (\zeta\sigma_x, \sigma_y), \tag{S12}$$

with $\zeta = \pm$ denoting the valley index, $\sigma_{x,y}$ the Pauli matrices in the usual representation and $\mathbf{q}_\zeta^\ell$ the momentum operator acting within the deformed moiré Brillouin zone

$$\mathbf{q}_\zeta^\ell = R\left[\pm\theta/2\right]\left(\mathbb{1} + \mathcal{E}^\ell\right)\left(\mathbf{q} - \mathbf{D}_\zeta^\ell\right), \tag{S13}$$

with the rotation matrix $R[\pm\theta]$

$$R[\pm\theta] = \begin{pmatrix} \cos\theta & \mp\sin\theta \\ \pm\sin\theta & \cos\theta \end{pmatrix}, \tag{S14}$$

with $\mathbf{q} = i\nabla$ and strain tensor $\mathcal{E}$,

$$\mathcal{E} = \epsilon \begin{pmatrix} (\nu\sin^2\phi - \cos^2\phi) & (1+\nu)\sin\phi\cos\phi \\ (1+\nu)\sin\phi\cos\phi & (\nu\cos^2\phi - \sin^2\phi) \end{pmatrix}. \tag{S15}$$

The positions of the Dirac points in each layer are given by

$$\mathbf{D}_\zeta^\ell = \left(\mathbb{1} - \mathcal{E}^\ell\right) R\left[\mp\theta/2\right] \mathbf{K}_\zeta - \zeta\mathbf{A}^\ell, \tag{S16}$$

where $\mathbf{K}_\zeta = -\zeta/3\,(2\mathbf{b}_1 + \mathbf{b}_2) = 2\pi\zeta(3a)^{-1}\,(-2,0)^{\mathrm{T}}$ with $\mathbf{b}_{1,2}$ being the reciprocal lattice vectors of the monolayer graphene. The vector potential is defined as $\mathbf{A}^\ell = \sqrt{3}\beta_G(2a)^{-1}\left(\epsilon_{xx}^\ell - \epsilon_{yy}^\ell\ , -2\epsilon_{xy}^\ell\right)^{\mathrm{T}}$, with the Grüneisen dimensionless parameter $\beta_G \approx 3.14$. For the experimentally relevant case of the uniaxial heterostrain along the k_x-axis (i.e. for $\phi = 0$ in Eq. (3)), the expression for the vector potential simplifies to $\mathbf{A}^{\uparrow,\downarrow} = \mp\mathbf{A}$, where

$$\mathbf{A} = \frac{\sqrt{3}}{4a}\beta_G\epsilon(1+\nu)\begin{pmatrix} 1 \\ 0 \end{pmatrix}. \tag{S17}$$

The off-diagonal blocks in Eq. (S11) describe the interlayer coupling between twisted graphene layers in terms of the Fourier expansion,

$$U = U_t + U_l e^{i\zeta\tilde{\mathbf{g}}_1\cdot\mathbf{r}} + U_r e^{i\zeta(\tilde{\mathbf{g}}_1+\tilde{\mathbf{g}}_2)\cdot\mathbf{r}}, \tag{S18}$$

with $\tilde{\mathbf{g}}_i$ defined in Eqs. (1), (12), and matrices

$$U_t = \begin{pmatrix} u & v \\ v & u \end{pmatrix}, \quad U_l = \begin{pmatrix} u & v\omega^{-\zeta} \\ v\omega^{\zeta} & u \end{pmatrix}, \quad U_r = \begin{pmatrix} u & v\omega^{\zeta} \\ v\omega^{-\zeta} & u \end{pmatrix},$$

with $\omega = \exp\{2\pi i/3\}$, $u = 0.0797$eV, and $v = 0.0975$eV. To diagonalize the Hamiltonian in Eq. (S11) we restrict the number of wave vectors in Eq. (S11). Without strain [12], the band structure can be accurately described with 91 wave vectors. However, as the strain increases, additional wave vectors are needed. The wave vectors are simply given by the linear combination $n\tilde{\mathbf{g}}_1 + m\tilde{\mathbf{g}}_2$ with n, m integers. The total number of vectors is set to be large enough to achieve convergence.

VI. THE RECIPROCAL LATTICE VECTORS AT THE CRITICAL STRAIN

From Eqs. (5) and Eq. (12), we get the reciprocal lattice vectors at the critical strain,

$$\tilde{\mathbf{g}}_{1,2} = \left(\mp\sqrt{3} - \frac{3}{\sqrt{\nu}}\right)\tilde{k}_0 \begin{pmatrix} 1 \\ \sqrt{\nu} \end{pmatrix}. \tag{S19}$$

Then, the linear combination of both vectors yields

$$n\tilde{\mathbf{g}}_1 + m\tilde{\mathbf{g}}_2 = \sqrt{3}\tilde{k}_0 \left[m - n - \sqrt{\frac{3}{\nu}}(n+m)\right] \begin{pmatrix} 1 \\ \sqrt{\nu} \end{pmatrix}. \tag{S20}$$

Obviously, the single periodicity condition requires

$$n\tilde{\mathbf{g}}_1 + m\tilde{\mathbf{g}}_2 = 0, \tag{S21}$$

or correspondingly

$$\frac{1}{\sqrt{\nu}} = \frac{1}{\sqrt{3}}\frac{m-n}{m+n}, \tag{S22}$$

from which Eq. (19) follows.

VII. EVOLUTION OF THE TBG BAND STRUCTURE WITH STRAIN

Figure S6 shows the evolution of the lower middle band of the twisted bilayer graphene as function of the strain. With increasing strain values, the cones move on complex trajectories thorough the moiré Brillouin zone [12–15]. The complexity of this trajectory is due to the interplay between energetic and geometric contributions, cf. Ref. [12]. In the process of approaching the critical strain, the bands of the initially two-dimensional system are gradually deformed and compressed down to those of an effective one-dimensional system. The analysis of the middle bands under strain reveals an intricate dynamics of their saddle points, cf. Fig. S7. At zero strain all three saddle points are located at the same energy, i.e. there is a three-fold saddle point degeneracy. This degeneracy is protected by the $\mathbf{C_3}$-symmetry between the saddle points in each of the bands, which is broken by the strain. This leads to the loss of the saddle point degeneracy and gives rise to a multiple peaked structure in the DOS, cf. Fig. S7. The strain reduces the $\mathbf{C}_3$-symmetry of the TBG moiré superlattice to the mere $\mathbf{C}_2$-symmetry. This reduction in the symmetry lifts all spectral degeneracies protected by the $\mathbf{C}_3$-symmetry, such as the positions of nodal and saddle points in the middle bands and similar spectral features of the remote bands, which are shifted with respect to each other on the energy axis. At the critical strain, the moiré Brillouin zone collapses to a line and the wave vectors become parallel to each other following Eq. (S20). For numerical diagonalization one needs to truncate the Hamiltonian at some finite size. The spectra obtained with different precision are shown in Fig. S8.

VIII. RELAXATION EFFECTS

For small twist angles θ, the geometrical deformations of the moiré unit cell discussed in the main text appear at very low strains of the order $\epsilon \sim \theta$. For the case of twisted bilayer graphene, the relaxation effects will shrink significantly

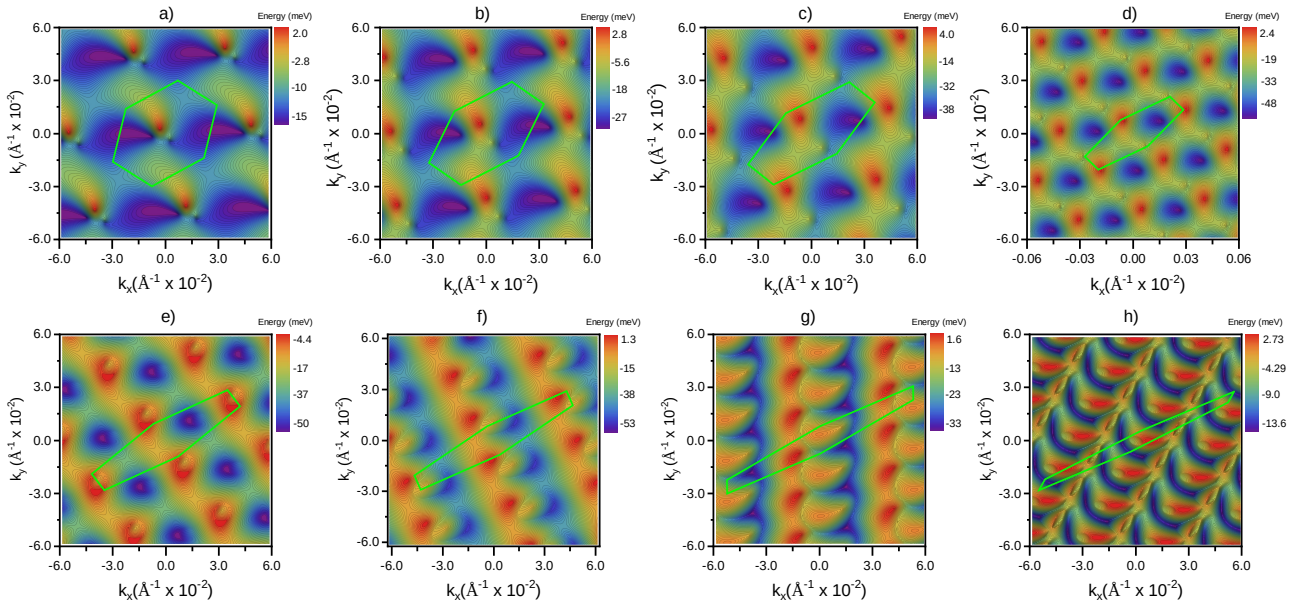

FIG. S6. Evolution of the bottom middle band of TBG with the twist angle $\theta = 1.0°$ as function of the strain for: a) $0.1\epsilon_c$, b) $0.2\epsilon_c$, c) $0.3\epsilon_c$, d) $0.4\epsilon_c$, e) $0.5\epsilon_c$ f) $0.6\epsilon_c$, g) $0.7\epsilon_c$ and h) $0.8\epsilon_c$; ϵ_c denotes the critical strain value defined in Eq. (6). Green hexagon emphasizes the moiré Brillouin zone.

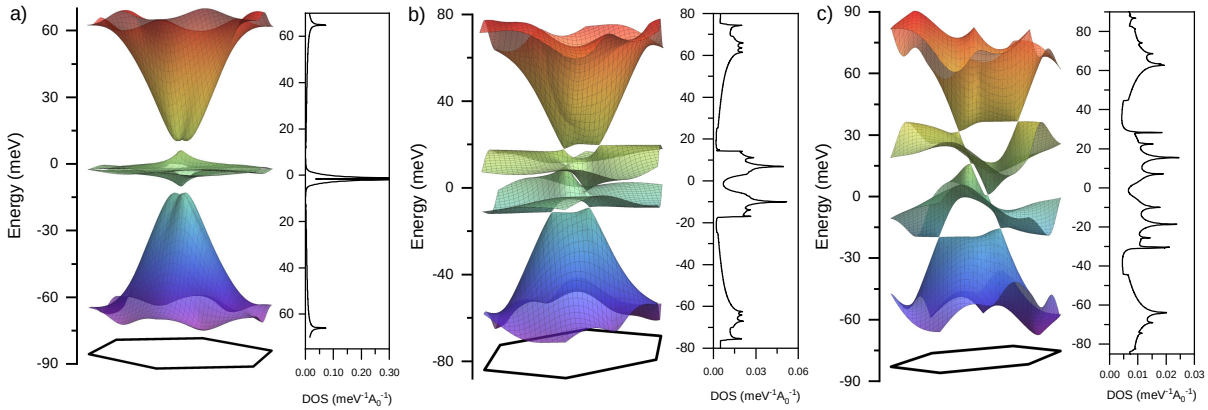

FIG. S7. Evolution of the band structure and DOS of TBG with the twist angle $\theta = 1.0°$ as a function of the uniaxial heterostrain with Poisson ratio $\nu = 0.165$ ($\epsilon_c \approx 4.4\%$) and: a) $\epsilon = 0\ \epsilon_c$, a) $\epsilon = 0.10\ \epsilon_c$, c) $\epsilon = 0.20\ \epsilon_c$. The corresponding moiré Brillouin zone is shown underneath each spectrum.

the AA-regions, leading to the formation of one-dimensional channels, see for instance Refs. [1, 16–18], where the low energy electron states are defined. It can be expected that, at the critical strain in the minimal angle regime, the twisted bilayer graphene would be described by a network of parallel one-dimensional channels.

[1] F. Guinea and N. R. Walet, Continuum models for twisted bilayer graphene: Effect of lattice deformation and hopping parameters, Phys. Rev. B **99**, 205134 (2019).
[2] P. San-Jose, J. González, and F. Guinea, Non-abelian gauge potentials in graphene bilayers, Phys. Rev. Lett. **108**, 216802 (2012).
[3] J. González, Confining and repulsive potentials from effective non-abelian gauge fields in graphene bilayers, Phys. Rev. B **94**, 165401 (2016).

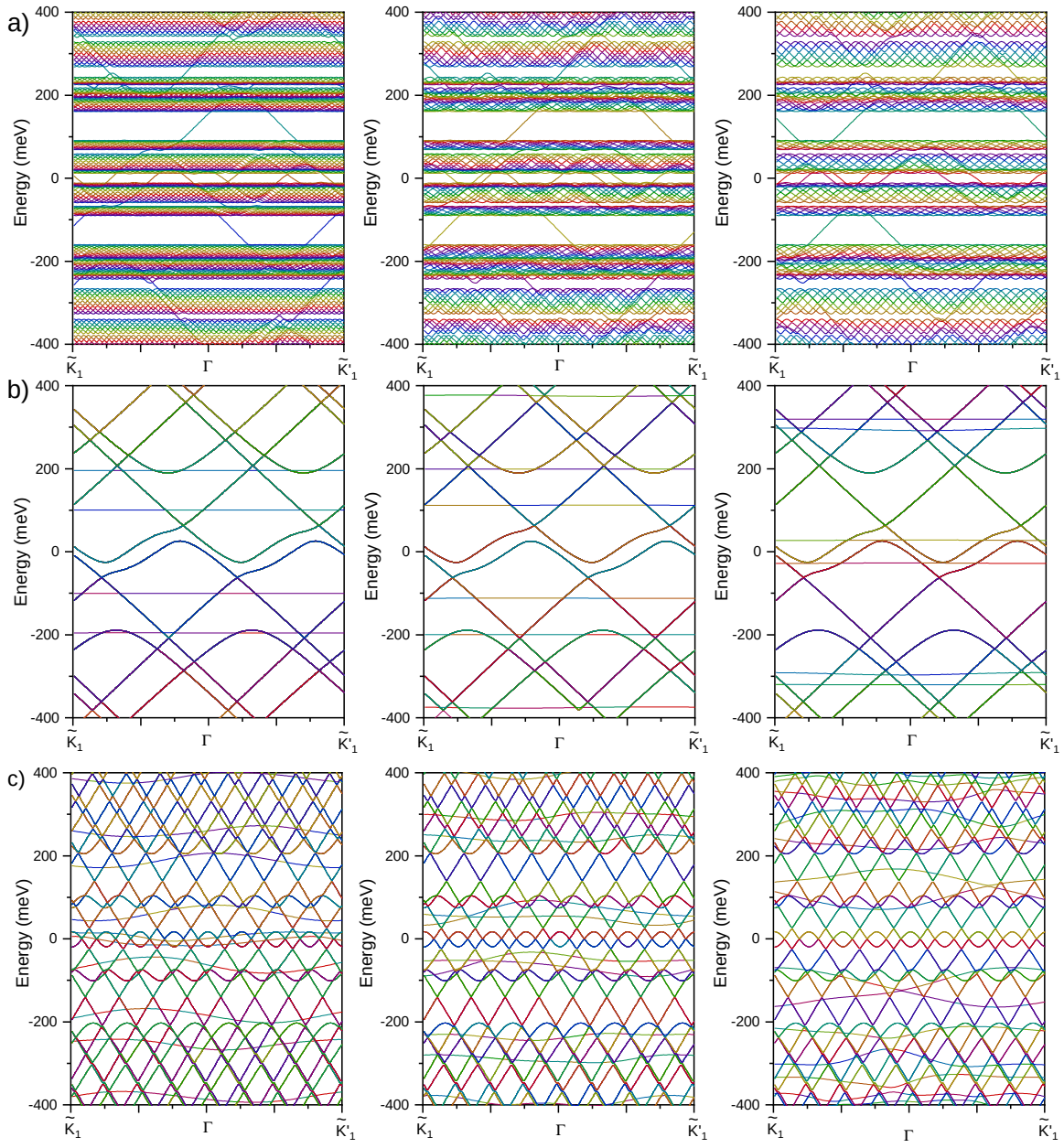

FIG. S8. Band structures of the critically strained TBG for $\theta = 1^\circ$ and different values of the ratio between applied strains, from top to bottom: a) $-\epsilon_{yy}/\epsilon_{xx} = 0.165$, b) $-\epsilon_{yy}/\epsilon_{xx} = 1/3$ and c) $-\epsilon_{yy}/\epsilon_{xx} = 1/12$. The spectra are evaluated along the collapsed moiré Brillouin zone depicted in Fig. (1). The columns are calculated with decreasing precision (from left to right) for the Hamiltonian Eqs. (S11)-(S18) truncated at 1951, 1261, and 721 $\tilde{\mathbf{g}}$-vectors in the reciprocal space. The convergence is almost reached in both cases with a single periodicity (middle and bottom rows). The spectrum of the $-\epsilon_{yy}/\epsilon_{xx} = 0.165$ realization (top row) reveals new structures at every higher precision, typical for aperiodical systems.

[4] A. Timmel and E. J. Mele, Dirac-harper theory for one-dimensional moiré superlattices, Phys. Rev. Lett. **125**, 166803 (2020).

[5] A. Timmel and E. J. Mele, Anomalous electrodynamics and quantum geometry in the dirac-harper model for a graphene bilayer, Phys. Rev. B **104**, 075419 (2021).

[6] D. A. Cosma, J. R. Wallbank, V. Cheianov, and V. I. Fal'ko, Moire pattern as a magnifying glass for strain and dislocations in van der waals heterostructures, Faraday Disc. **173**, 137 (2014).

[7] V. o. T. Phong and E. J. Mele, Obstruction and interference in low-energy models for twisted bilayer graphene, Phys. Rev. Lett. **125**, 176404 (2020).

[8] L. Molino, L. Aggarwal, V. Enaldiev, R. Plumadore, V. Falko, and A. Luican-Mayer, Ferroelectric switching at symmetry-broken interfaces by local control of dislocation networks, arXiv 10.48550/arxiv.2210.03074 (2022), arXiv:2210.03074.

[9] J. M. B. Lopes dos Santos, N. M. R. Peres, and A. H. Castro Neto, Graphene bilayer with a twist: Electronic structure, Phys. Rev. Lett. **99**, 256802 (2007).

[10] R. Bistritzer and A. H. MacDonald, Moiré bands in twisted double-layer graphene, Proceedings of the National Academy of Sciences **108**, 12233 (2011).

[11] J. M. B. Lopes dos Santos, N. M. R. Peres, and A. H. Castro Neto, Continuum model of the twisted graphene bilayer, Phys. Rev. B **86**, 155449 (2012).

[12] P. A. Pantaleón, V. o. T. Phong, G. G. Naumis, and F. Guinea, Interaction-enhanced topological hall effects in strained twisted bilayer graphene, Phys. Rev. B **106**, L161101 (2022).

[13] Z. Bi, N. F. Q. Yuan, and L. Fu, Designing flat bands by strain, Physical Review B **100**, 10.1103/physrevb.100.035448 (2019).

[14] P. A. Pantaleón, T. Low, and F. Guinea, Tunable large berry dipole in strained twisted bilayer graphene, Phys. Rev. B **103**, 205403 (2021).

[15] L. Zhang, Y. Wang, R. Hu, P. Wan, O. Zheliuk, M. Liang, X. Peng, Y.-J. Zeng, and J. Ye, Correlated states in strained twisted bilayer graphenes away from the magic angle, Nano Letters **22**, 3204 (2022).

[16] D. K. Efimkin and A. H. MacDonald, Helical network model for twisted bilayer graphene, Phys. Rev. B **98**, 035404 (2018).

[17] N. R. Walet and F. Guinea, The emergence of one-dimensional channels in marginal-angle twisted bilayer graphene, 2D Materials **7**, 015023 (2019).

[18] C. De Beule, F. Dominguez, and P. Recher, Aharonov-bohm oscillations in minimally twisted bilayer graphene, Phys. Rev. Lett. **125**, 096402 (2020).